

Article

Effect of Surface Wettability on Nanoparticle Deposition during Pool Boiling on Laser-Textured Copper Surfaces

Jure Berce ¹, Armin Hadžić ¹, Matic Može ¹, Klara Arhar ¹, Henrik Gjerkeš ², Matevž Zupančič ¹
and Iztok Golobič ^{1,*}

¹ Faculty of Mechanical Engineering, University of Ljubljana, Aškerčeva 6, 1000 Ljubljana, Slovenia; jure.berce@fs.uni-lj.si (J.B.); armin.hadzic@fs.uni-lj.si (A.H.); matic.moze@fs.uni-lj.si (M.M.); klara.arhar@fs.uni-lj.si (K.A.); matevz.zupancic@fs.uni-lj.si (M.Z.)

² School of Engineering and Management, University of Nova Gorica, Vipavska 13, 5000 Nova Gorica, Slovenia; henrik.gjerkes@ung.si

* Correspondence: iztok.golobic@fs.uni-lj.si; Tel.: +386-1-4771-420

Abstract: Prior studies have evidenced the potential for enhancing boiling heat transfer through modifications of surface or fluid properties. The deployment of nanofluids in pool boiling systems is challenging due to the deposition of nanoparticles on structured surfaces, which may result in performance deterioration. This study addresses the use of TiO₂–water nanofluids (mass concentrations of 0.001 wt.% and 0.1 wt.%) in pool boiling heat transfer and concurrent mitigation of nanoparticle deposition on superhydrophobic laser-textured copper surfaces. Samples, modified through nanosecond laser texturing, were subjected to boiling in an as-prepared superhydrophilic (SHPI) state and in a superhydrophobic state (SHPO) following hydrophobization with a self-assembled monolayer of fluorinated silane. The boiling performance assessment involved five consecutive boiling curve runs under saturated conditions at atmospheric pressure. Results on superhydrophilic surfaces reveal that the use of nanofluids always led to a deterioration of the heat transfer coefficient (up to 90%) compared to pure water due to high nanoparticle deposition. The latter was largely mitigated on superhydrophobic surfaces, yet their performance was still inferior to that of the same surface in water. On the other hand, CHF values of 1209 kW m⁻² and 1462 kW m⁻² were recorded at 0.1 wt.% concentration on both superhydrophobic and superhydrophilic surfaces, respectively, representing a slight enhancement of 16% and 27% compared to the results obtained on their counterparts investigated in water.

Keywords: nanoparticles; nanoparticle deposition; nanofluids; laser texturing; hydrophobization; boiling heat transfer



Citation: Berce, J.; Hadžić, A.; Može, M.; Arhar, K.; Gjerkeš, H.; Zupančič, M.; Golobič, I. Effect of Surface Wettability on Nanoparticle Deposition during Pool Boiling on Laser-Textured Copper Surfaces. *Nanomaterials* **2024**, *14*, 311. <https://doi.org/10.3390/nano14030311>

Academic Editors: Florian Ion Tiberiu Petrescu, Manuel M. Piñeiro and Gang Shi

Received: 23 December 2023

Revised: 16 January 2024

Accepted: 1 February 2024

Published: 4 February 2024



Copyright: © 2024 by the authors. Licensee MDPI, Basel, Switzerland. This article is an open access article distributed under the terms and conditions of the Creative Commons Attribution (CC BY) license (<https://creativecommons.org/licenses/by/4.0/>).

1. Introduction

Pool boiling, recognized for its exceptional efficacy of heat dissipation, has found application in various industrial systems, including air conditioning [1,2], heat exchangers [3–5], domestic refrigerators [6,7], spacecraft thermal management [8,9], and high-power electronics cooling [10–13]. In recent decades, various cooling methodologies have been advanced for the purpose of heat dissipation, encompassing techniques involving porous media, microchannel heat sinks, spray cooling, as well as natural and forced convection, among others. Among these approaches, pool boiling has emerged as a notably efficient method, demonstrating superior heat dissipation efficacy compared to prevalent contemporary cooling techniques. Notably, a select few, namely, spray cooling, microchannel heat sinks, and heat removal techniques involving porous media, exhibit comparable or slightly lower efficiency levels within the spectrum of contemporary cooling technologies [13–15]. However, the present demands of increased heat removal capacities, coupled with the imperative for enhanced efficiency in heat transfer systems, give rise to a notable challenge. In response to this challenge, recent research efforts have concentrated on augmenting key parameters

of boiling heat transfer, specifically the heat transfer coefficient (HTC) and critical heat flux (CHF). The latter represents the upper limit of nucleate boiling, manifesting when the surface is covered with an excessive population of bubbles at high heat flux, leading to extensive coalescence and the formation of an insulating vapor blanket. This blanket significantly reduces heat transfer intensity. The heat transfer coefficient is defined as the ratio between dissipated heat flux and the corresponding wall superheat, denoting the temperature differential between the boiling surface and the bulk fluid. HTC is calculated by the following equation:

$$h = \frac{\dot{q}}{T_w - T_{sat}} \quad (1)$$

In Equation (1), \dot{q} presents the heat flux, while T_w presents the calculated surface temperature and T_{sat} presents the saturation temperature of the bulk fluid.

To enhance boiling performance, one method involves manipulating the thermophysical properties of the boiling fluid, often achieved by adding nanoparticles to the base fluid, thereby forming nanofluids [16,17]. While certain studies have demonstrated improved boiling performance with nanofluids, challenges arise in controlling the thickness of deposited nanoparticles on surfaces, causing added thermal resistance and deterioration of heat transfer, resembling particulate fouling [18,19]. Addressing this, various parameters such as nanoparticle concentration [20,21], type [22,23], size [24], and deposition time during boiling [25,26] have been investigated to optimize heat transfer performance. Higher concentrations result in a reduction in HTC, attributed to elevated thermal resistance due to the growth of the deposited layer on the surface [27,28]. Furthermore, studies focused on the investigation of the effect of nanofluid boiling time demonstrated that an increase in nanofluid boiling time results in the formation of a deposited nanoparticle layer, leading to a reduction in contact angle and an increase in CHF [16,29]. However, it was also reported that the deposition of nanoparticles on the heated surface decreased the boiling HTC due to the rise in thermal resistance [15,29].

In addition to concentration and deposition time, the material and size of nanoparticles, as well as nanofluid preparation, influence boiling efficiency. Dadhich et al. [30] and Fang et al. [28] highlighted the considerable necessity for a comprehensive database encompassing thermal properties across various materials and nanoparticle size ranges. Moreover, we previously showed [29] that nanofluids with small (4–8 nm) and large (490 nm) nanoparticles lead to the deterioration of HTC on copper surfaces with laser-induced structure in comparison to the results obtained with pure water on laser-engineered surfaces. The deterioration of HTC was more pronounced with the utilization of larger nanoparticles, which was mainly attributed to the filling of laser-induced microcavities with particles that are approximately similar in size. One of the most promising ways to utilize nanofluid to have a positive effect on heat transfer efficiency in boiling systems is to reduce the deposition rates of nanoparticles on boiling surfaces.

Furthermore, a more promising method for enhancing boiling heat transfer involves tailoring surface morphology and topology. Various techniques, including electrochemical processes [31,32], chemical vapor deposition [33], laser texturing [34,35], and wet/dry etching [36], have been employed to fabricate surfaces with porous structures [37], micropin fins [38], nanowire and nanoflower structures [39], and microcavities [40] on boiling interfaces. Surfaces with tailored interfaces have demonstrated increased CHF due to augmented liquid supply. Moreover, altering surface wettability has been explored to improve liquid supply, thereby enhancing CHF and HTC. Hydrophilic surfaces have been associated with higher CHF values, while surfaces with opposite wetting properties reduce the energy barrier for nucleate boiling onset, leading to improved HTCs, especially at low and medium heat fluxes. However, such surfaces are incapable of limiting bubble merging, which leads to a lower CHF value compared to surfaces with better wetting properties. Nevertheless, recent research findings presented by Allred et al. [41] and Može et al. [40] demonstrate that significant enhancement of HTC can be achieved on adequately degassed superhydrophobic surfaces, without causing a drastic reduction in CHF. Furthermore, sur-

faces denoted as “(super)biphilic” that exhibit heterogeneous wettability with juxtaposed hydrophilic and hydrophobic regions have the aim of manipulating nucleation phenomena while considering the interplay of liquid and vapor flows, which can lead to simultaneous enhancement of HTC and CHF [42–45].

The surfaces with tailored wettability and their effect on boiling performance are mostly tied to tests with pure water. Although there are several studies that have tested nanofluid boiling performance on structured surfaces with tailored wetting properties, structured surfaces that exhibited a superhydrophilic wetting state demonstrated the greatest critical heat flux, but also the deterioration of HTC, due to filling the artificial cavities with nanoparticles, resulting in reduced nucleation site density [29,46]. Furthermore, Freitas et al. [47] investigated the pool boiling performance and bubble dynamics of nanofluids on biphilic surfaces. The low-wettable areas enable the control of bubble merging, while the highly wettable surroundings promote the liquid supply, contributing to the cooling of the surface. Furthermore, they showed that low-concentrated nanofluids have a minor influence on bubble dynamics and heat transfer efficiency during boiling. Ultimately, a single study, published by Ji et al. [48], was identified as having previously integrated surfaces possessing hydrophobic and superhydrophobic properties with the utilization of nanofluids to augment boiling heat transfer. For the superhydrophobic surface with higher roughness (contact angle 153.0°), boiling heat transfer was enhanced at a heat flux less than 93 kW m^{-2} , and then the heat transfer degraded at a higher heat flux.

There is limited research examining the boiling performance of nanofluids on laser-functionalized surfaces with tailored wettability, despite the seemingly great potential for enhancement of boiling performance and the possibility of mitigating the deposition of nanoparticles during nanofluid boiling by tailoring the wettability of the structured surfaces. In an effort to address this gap, we conducted an examination of the pool boiling performance of TiO_2 -water nanofluids at two mass concentrations (0.001 and 0.1 wt.%) of nanoparticle sizes of 4–8 nm, on superhydrophilic and superhydrophobic laser-textured copper surfaces. Five consecutive pool boiling curve measurements were performed on each surface at atmospheric pressure. Laser-functionalized surfaces were developed utilizing nanosecond laser texturing, followed by the application of hydrophobic monolayer coating using a 3 mM solution of 2-propanol and fluorinated alkyl phosphonic acid. To clarify the effect of nanoparticle deposition on boiling performance, surface characteristics after boiling tests with nanofluids were analyzed using contact angle measurements and scanning electron microscopy.

2. Materials and Methods

2.1. Surface Preparation and Analysis

High-purity copper samples (>99.9%) were used to perform the pool boiling experiments. The top part of the samples served as a boiling interface, which was first sanded with sandpapers P1200 and P2000, and then cleaned with 2-propanol prior to testing or subsequent treatment. The achieved roughness (Ra) of the sanded samples was approximately $0.2 \mu\text{m}$. The surface roughness of the tested samples was measured using a Mitutoyo SJ-310 device (Mitutoyo Corporation, Kanagawa, Japan). Among the tested samples, one was tested without any further treatment and served as a reference surface, while other samples underwent further functionalization of the boiling interface.

The first step in functionalizing surfaces was laser texturing performed with a nanosecond fiber laser (JPT Opto-electronics Co., Ltd., Shenzhen, China, M7 30 W MOPA; $\lambda = 1064 \text{ nm}$). The laser beam was directed across the surface with an F-Theta lens with a working area of $70 \times 70 \text{ mm}^2$ and a focal distance of 100 mm. The focused beam spot diameter was approx. $25 \mu\text{m}$, the laser beam quality $M^2 < 1.3$ (manufacturer data), and the maximal power of the laser source was 30 W. Surface treatment patterns were designed in ezCAD 2 software, which was also used to control the laser system during the laser treatment. The microstructure on surfaces was fabricated utilizing a pattern of equidistant parallel lines

($\Delta x = 60 \mu\text{m}$) with the following laser processing parameters: pulse duration of 45 ns, pulse frequency of 110 kHz, and maximum laser power of 30 W.

Three samples after laser texturing underwent further functionalization that included hydrophobization utilizing a solution of 3,3,4,4,5,5,6,6,7,7,8,8,9,9,10,10,11,11,12,12,12-henicosafuorododecylphosphonic acid (abbreviated to FDPA, CAS Nr. 252237-39-1, abcr GmbH product code AB254085). FDPA was dissolved in 2-propanol (Honeywell, ACS reagent, Charlotte, NC, USA, $\geq 99.5\%$) at a concentration of 3 mM. The hydrophobization process of the surfaces was performed by pipetting three drops of FDPA solution onto the sample. Furthermore, samples were left to dry at room temperature for 5 min, then in the oven at 80 °C for another 15 min.

The collection of surfaces and boiling fluids prepared and tested within the study is summarized in Table 1.

Table 1. Summary of tested working fluids and surfaces within this study.

| Sample Name | Working Fluid | Concentration (wt.%) | Static Contact Angle (°) | |
|-------------|-------------------------|----------------------|--------------------------|---------------|
| | | | Before Boiling | After Boiling |
| REF | Water | / | 61 | 93 |
| SHPI | Water | / | 0 | 110 |
| SHPO | Water | / | 164 | 148 |
| SHPI-0.001% | TiO ₂ -water | 0.001 | 0 | 17 |
| SHPI-0.1% | TiO ₂ -water | 0.1 | 0 | 0 |
| SHPO-0.001% | TiO ₂ -water | 0.001 | 164 | 79 |
| SHPO-0.1% | TiO ₂ -water | 0.1 | 164 | 20 |

The examination of functionalized surface properties involved utilizing scanning electron microscopy (SEM) and contact angle measurements. To analyze the micro- and nanostructure of the surfaces, a scanning electron microscope (ThermoFisher Scientific Quattro S, Waltham, MA, USA) was employed, employing both backscattered electron (BSE) and secondary electron (SE) imaging at an accelerating voltage of 10 kV. Figure 1 shows SEM images of the untreated and laser-engineered surfaces before they underwent boiling tests. Contact angle measurements were conducted using a goniometer (Ossila, Sheffield, UK), and the assessments were carried out with twice-distilled water at room temperature. These measurements were performed on the prepared and tested samples both immediately before and after the boiling test within the scope of this study. The static contact angle results for the tested surfaces are presented in Table 1.

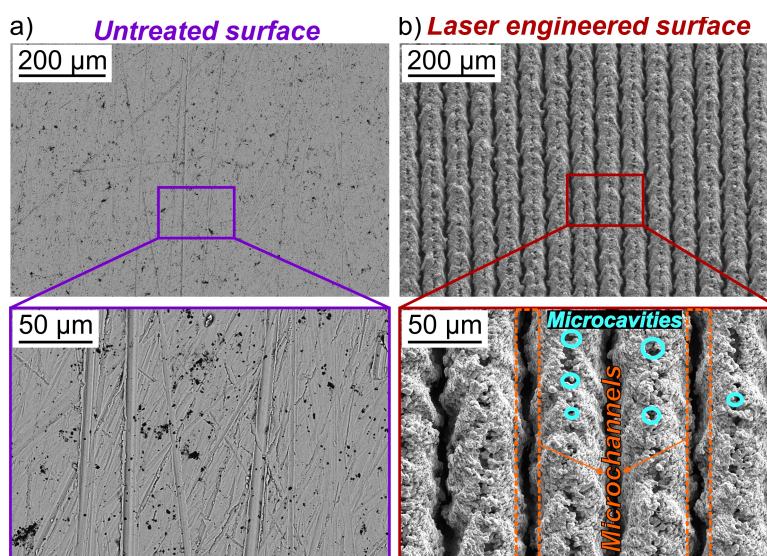


Figure 1. SEM images of the reference samples: (a) untreated surface and (b) laser-engineered surface.

2.2. Nanofluid Preparation

The titanium dioxide-water nanofluids employed in this investigation were prepared using twice-distilled water, previously degassed utilizing vigorous boiling, and TiO₂ nanoparticles. The stability of nanofluid solutions was maintained by utilizing ultrasonic vibration. The selection of TiO₂ nanoparticles for this study was motivated by their commendable chemical and physical stability, coupled with their hydrophilic properties, previously observed to augment the critical heat flux (CHF) value in boiling experiments, which could be helpful to the augmentation of CHF on superhydrophobic surfaces, due to their known characteristic of decreasing the CHF.

The nanofluid solutions consisted of small nanoparticles, ranging in size from 4 to 8 nm (Carl Roth, Karlsruhe, Germany; ROTInanoMETIC \geq 99.9%), and were prepared at two distinct mass concentrations: 0.1 and 0.001 wt.%. Before the preparation of each solution, 100 mL of twice-distilled water underwent degassing for 45 min through vigorous boiling to mitigate the presence of non-condensable gases. In the first step of nanofluid preparation for both concentrations, twice the amount of nanoparticles was dispersed in 100 mL of degassed twice-distilled water. Subsequently, the nanofluids underwent one hour of sonication immediately after preparation in an ultrasonic bath (ASonic, Ultrasonic Cleaner-Pro 30, 40 kHz, 120 W) to ensure homogeneity and mitigate the potential for irregularities in the distribution of nanoparticles. The other 100 mL of twice-distilled water was used for the degassing of the superhydrophobic surface and removing entrapped gasses from surface cavities. This protocol of degassing both the surface and the solution removed the need for using the nanofluid solution for degassing within the boiling chamber and the possible reduction of nanoparticle concentration due to their deposition on the immersion heater. The final nanofluid solutions of 200 mL with concentrations of 0.001 wt.% and 0.1 wt.% were produced by mixing 100 mL of double-concentrated, previously prepared nanofluid solutions into 100 mL of twice-distilled water within the boiling chamber.

2.3. Experimental Setup

The assessment of boiling performance on laser-textured surfaces with tailored wettability was conducted through the utilization of a previously established experimental setup, depicted in Figure 2. Boiling tests were performed utilizing a glass boiling chamber with an inner diameter of 60 mm. The working fluid temperature was monitored using two submerged K-type thermocouples at varying heights within the chamber. A condenser, cooled by a secondary water loop, was positioned atop the assembly to maintain a consistent water level during experiments. Temperature signals were recorded as raw voltages at a rate of 10 Hz, employing a DAQ device (KRYPTIONi-8xTH; Dewesoft, Trbovlje, Slovenia) and Dewesoft X3 2022.1 software. Further details about the experimental setup can be found in our previous work [29,43].

2.4. Data Reduction and Measurement Uncertainty

Altogether, five temperatures were measured during the experiment—three inside the sample and two in the water. From these, the heat flux, surface superheat, and heat transfer coefficient were calculated and recorded in real time with the DewesoftX3 2022.1 software, while the post-processing was conducted with Mathworks MATLAB R2021a. The flowchart of data post-processing conducted with MATLAB is presented in Figure 3. More details are available in our previous work [43,49].

Briefly, the temperature-dependent thermal conductivity was determined at the average sample temperature, calculated as the arithmetic mean of three thermocouple measurements. The heat flux was computed using Fourier's law of one-dimensional heat conduction, utilizing the temperature gradient derived from the thermocouple readings. Surface superheat was derived as the difference between the sample surface and water temperatures. The latter was determined as the arithmetic mean of both submerged thermocouple measurements, while the surface temperature was estimated using the measurement

closest to the surface (upper sample thermocouple) and the heat flux. The heat transfer coefficient was then obtained by dividing the heat flux by the surface superheat.

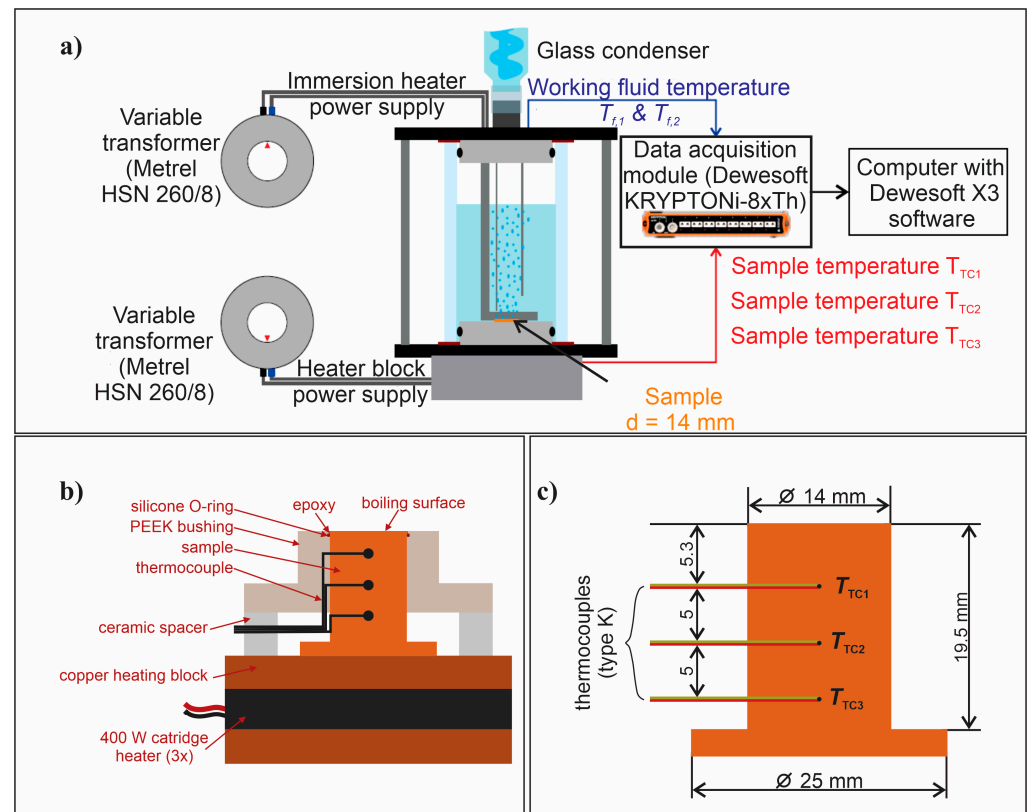


Figure 2. (a) Experimental setup; (b) cross section of the sample and the heating assembly; and (c) dimensions of the sample, including the position of thermocouples.

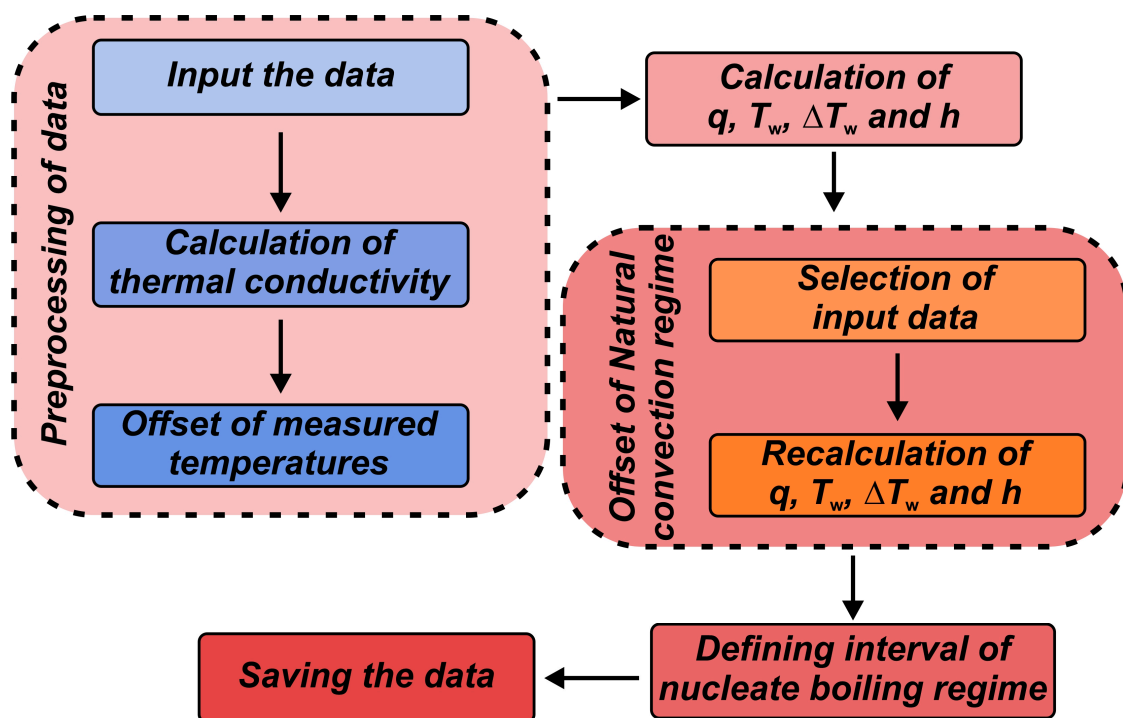


Figure 3. Flowchart of processing the data obtained during pool measurements.

The measurement uncertainty of heat transfer parameters is presented in Table 2.

Table 2. Measurement uncertainty.

| Heat Flux Level (kW m^{-2}) | Heat Flux (%) | Heat Transfer Coefficient (%) | Surface Superheat (K) |
|---|------------------|----------------------------------|--------------------------|
| 250 | 9–11 | 10–13 | 0.4 |
| 1000 | 5 | 12–16 | 0.8 |

2.5. Measurement Procedure

Boiling experiments for every combination of working fluid and surface featuring customized wettability comprised five runs. Each run involved recording the boiling curves up to the CHF, spanning a duration of 45 min. Throughout the boiling curve recording, the heat flux was slowly increased, following the methodology outlined by Može et al. [50]. Upon reaching CHF, the experimental run was completed, and the surface was allowed to cool down below $90\text{ }^{\circ}\text{C}$, which lasted approximately 15 min. Overall, the whole boiling test of a given sample was completed in a 5 h period.

3. Results

3.1. Pool Boiling Heat Transfer in Water

The evaluation of the boiling performance of the reference surface (REF) using twice-distilled water as a working fluid is shown in Figure 4. The untreated reference surface represents the initial state prior to any further functionalization. The highest CHF on untreated surfaces was 1084 kW m^{-2} and the highest HTC of $51\text{ kW m}^{-2}\text{ K}^{-1}$ at CHF was recorded during the fifth experimental run. During five repetitions of boiling tests on untreated surfaces, the shift of boiling curves towards lower superheat was observed. A 4.3 K reduction of surface superheat at high heat flux level (800 kW m^{-2}) near CHF was recorded, which can be attributed to the change of wetting state of the reference surface, i.e., from hydrophilic (contact angle of 61°) to hydrophobic (contact angle of 93°) after exposure to boiling.

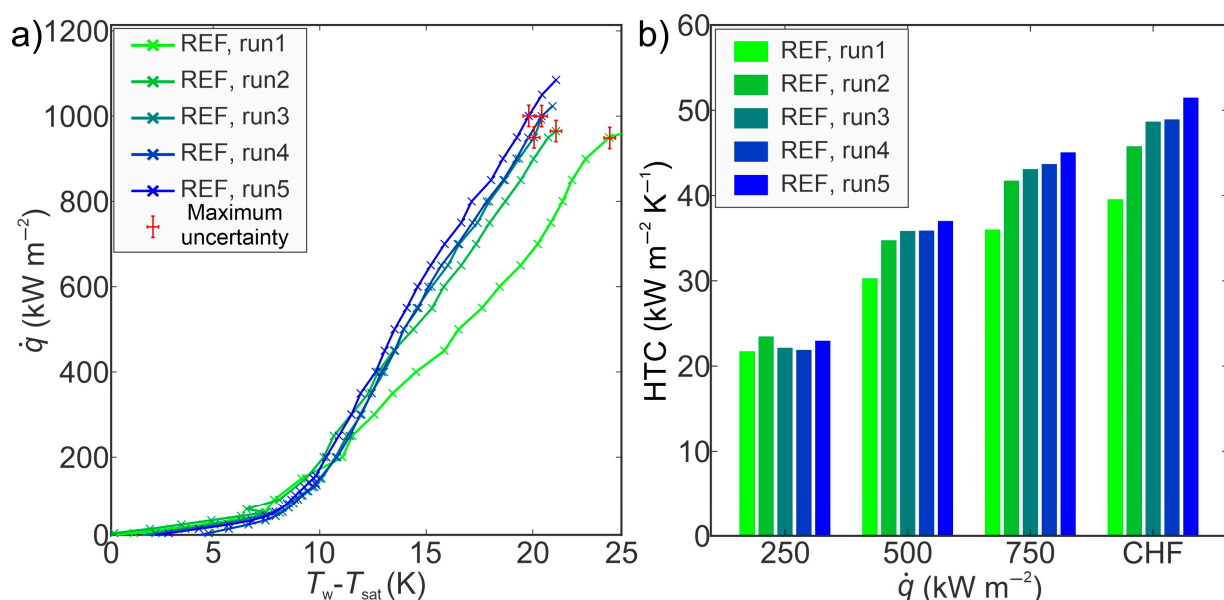


Figure 4. (a) Boiling curves and (b) heat transfer coefficients on the reference surface.

Figure 5 shows the boiling performance (Figure 5a—boiling curves and Figure 5b—heat transfer coefficients at different heat flux levels) obtained on a superhydrophilic laser-engineered surface. Laser texturing of untreated copper surfaces forms microchannels

and microcavities, which can serve to enhance liquid supply and increase nucleation site density, respectively [43,51]. The highest CHF of 1152 kW m^{-2} was recorded during the first experimental run. At CHF, the largest HTC value of $128 \text{ kW m}^{-2} \text{ K}^{-1}$ was recorded, and an enhancement over the reference surface of 150% was calculated. The remarkable enhancement of HTC can be attributed to the occurrence of secondary boiling effects near the CHF, leading to a significant reduction of surface superheat. The incipience of secondary boiling effects can be the result of the increase in the number of nucleation sites at high heat flux levels, where bubbles begin to nucleate not just within microcavities, but also on the peaks of the laser structure [43,52]. Moreover, the shift of the boiling curve towards lower superheats was also observed, with a 3.3 K reduction of superheat recorded at heat flux near the CHF (800 kW m^{-2}). This is the result of surface chemistry transformation occurring at high temperatures after reaching the first CHF during film boiling, as shown by Može et al. [53].

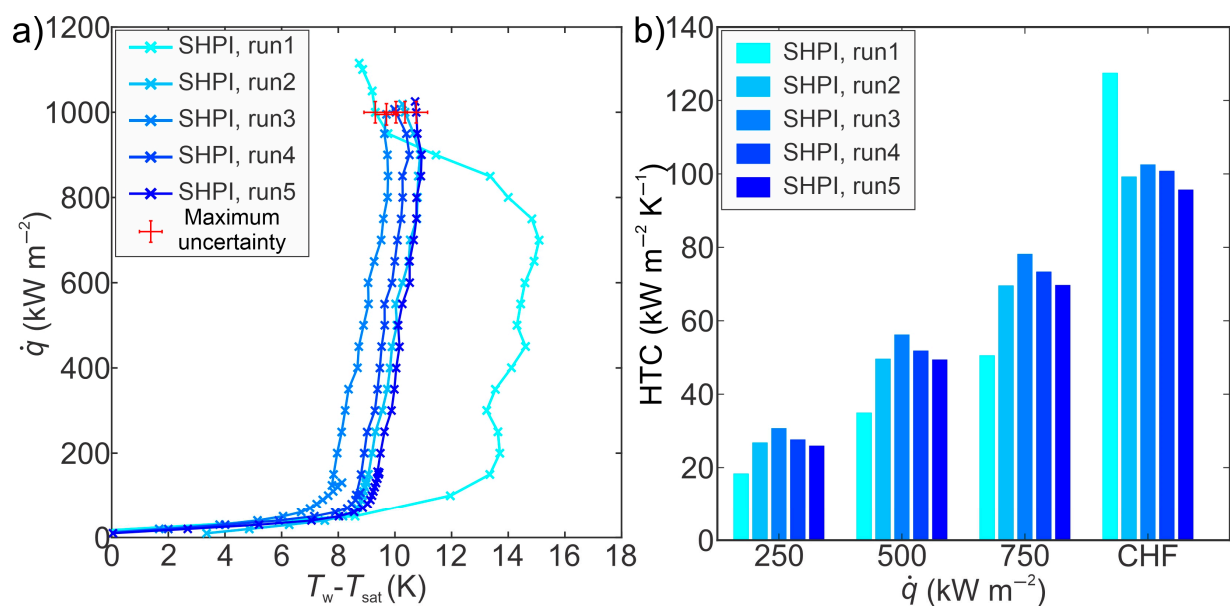


Figure 5. (a) Boiling curves and (b) heat transfer coefficients on the superhydrophilic laser-textured surface.

Figure 6 shows the boiling performance (Figure 6a—boiling curves and Figure 6b—HTCs at different heat flux levels) obtained on a superhydrophobic laser-engineered surface. Laser-induced cavities on the surface act as favored locations for nucleation during the boiling process, especially after the hydrophobization process. The static contact angle of $164^\circ \pm 0.7^\circ$ was recorded on superhydrophobic surfaces before boiling tests, while after exposure to boiling, a value of $140^\circ \pm 0.8^\circ$ was measured. The highest HTC of $108 \text{ kW m}^{-2} \text{ K}^{-1}$ at CHF was obtained during the third experimental run, with an enhancement of 112% over the reference surface. The average HTC of $97 \text{ kW m}^{-2} \text{ K}^{-1}$, obtained on superhydrophobic surfaces during five boiling tests, was similar to the average HTC ($99 \text{ kW m}^{-2} \text{ K}^{-1}$) recorded on a superhydrophilic (SHPI) surface. The shift of boiling curves towards lower superheat was also observed on the superhydrophobic (SHPO) surface, with a 0.2 K reduction of surface superheat at a heat flux of 500 kW m^{-2} from the first to the fifth experimental run. On the other hand, at the same heat flux values, a 3.9 K reduction of superheat was recorded on a superhydrophilic surface, indicating that the SHPO sample is significantly more stable than the SHPI surface. The CHF values during the five boiling tests were similar to the CHF values obtained on the reference surface.

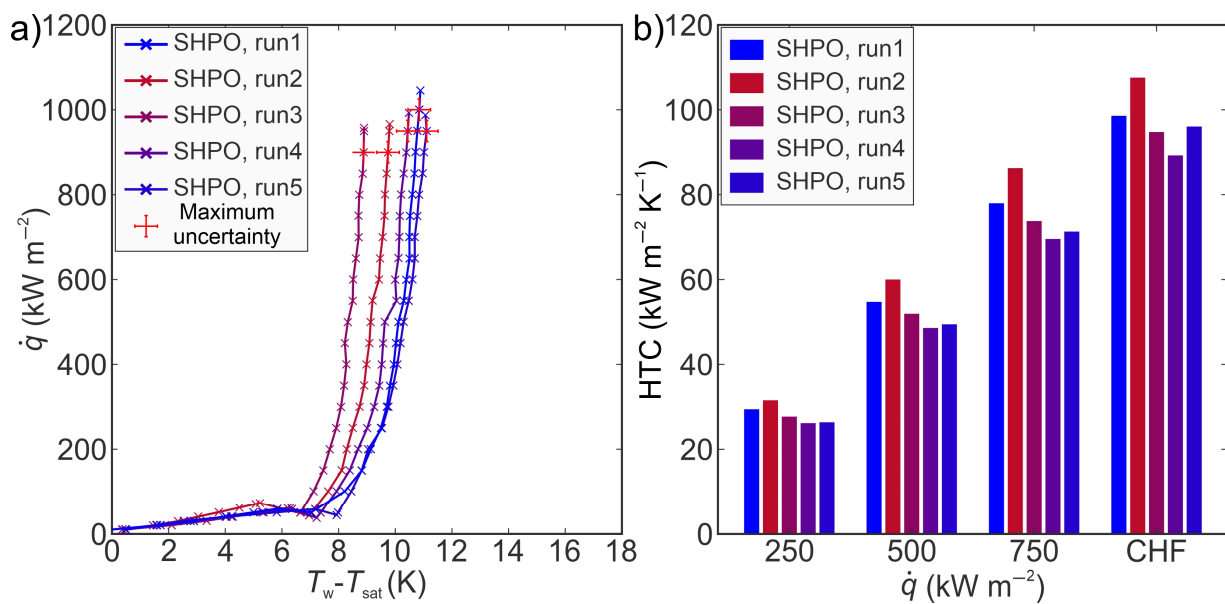


Figure 6. (a) Boiling curves and (b) heat transfer coefficients on the superhydrophobic laser-textured surface.

3.2. Boiling Heat Transfer on Superhydrophilic Surfaces with TiO₂–Water Nanofluid

Boiling curves recorded on a superhydrophilic laser-engineered surface using TiO₂ water nanofluid at two distinct concentrations are shown in Figure 7. Boiling curves obtained with lower concentrations were stable, and an increase in CHF of 35% from the first to the fifth experimental run was observed. On the other hand, boiling curves obtained with higher concentrations were unstable, and they shifted toward higher superheats with a low increase of CHF from the first to the second experimental run, followed by a decrease from the second to the fifth experimental run. The shift towards higher superheats obtained for the 0.1 wt.% nanofluid can be attributed to decreasing nucleation site density due to the deposition of nanoparticles in microcavities with each consecutive run. At high nanoparticle concentrations, the deposited layer on the surface becomes thicker, which leads to greater thermal resistance and decreases the HTC. However, the highest CHF of 1462 kW m⁻² was recorded at higher concentrations, representing an improvement of 35% compared to the highest CHF obtained on the reference sample. The CHF values obtained at 0.1 wt.% were higher compared to the CHF values achieved at 0.001 wt.%, which can be attributed to better wetting properties (i.e., the static contact angle recorded on the surface after boiling with 0.1 wt.% nanofluid was around 3°, while on the surface after boiling, 0.001% wt.% nanofluid was 110°). The observed effect of concentration on CHF is in agreement with the findings presented in the literature [29,54].

Heat transfer coefficients obtained at various heat flux levels on superhydrophilic laser-engineered surfaces employing TiO₂–water nanofluid at 0.001 and 0.1 wt.% concentrations are presented in Figure 8. The findings indicate that the heat transfer coefficients during five consecutive experimental runs at 0.001 wt.% remain remarkably consistent, exhibiting no discernible alterations. In contrast, the boiling performance at 0.1 wt.% shows a pronounced deterioration from the first to the fifth run. This decrease can be predominantly attributed to a reduction in nucleation site density on the structured surface, stemming from the deposition of nanoparticles onto the surface, or more precisely, filling the laser-induced microcavities, and thus influencing boiling performance. Furthermore, the disparities in boiling performance over an extended boiling duration at different concentrations can be attributed to the quantity of nanoparticles present in the nanofluid capable of being deposited onto the surface during boiling. Consequently, the initial experimental run at 0.1 wt.% reveals an increased deposition of nanoparticles on the surface, effectively filling more laser-induced cavities and forming a thicker nanoparticle layer compared to the

surface after the first experimental run at 0.001 wt.%. Following five hours of boiling at both concentrations, a substantial contrast in the deposited nanoparticle layers on the tested surfaces became apparent.

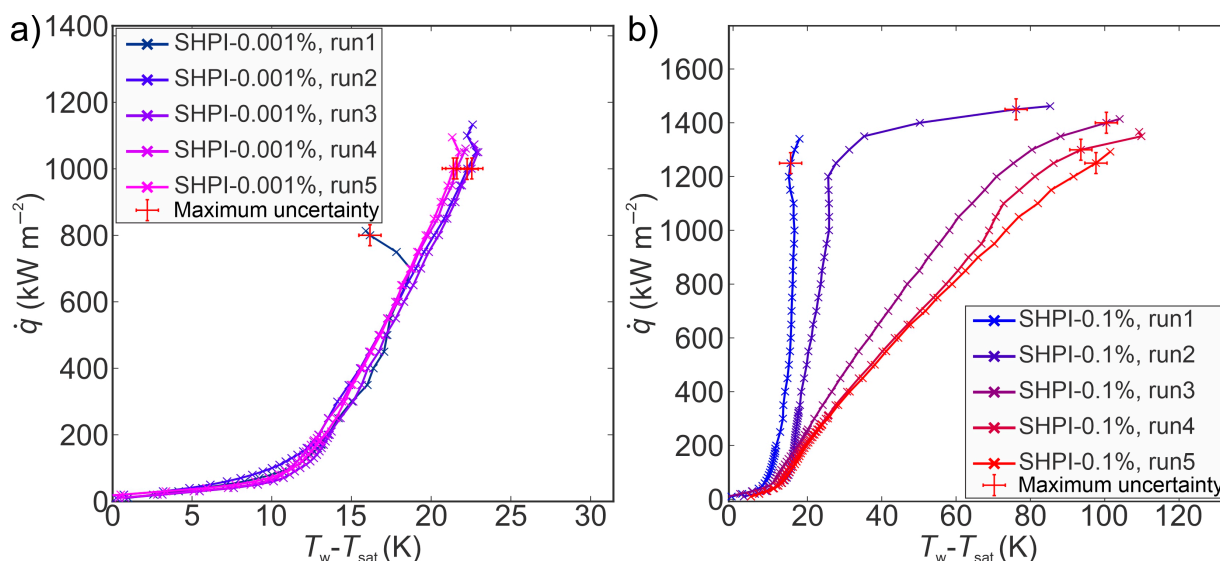


Figure 7. Boiling curves of TiO₂–water nanofluid on a superhydrophilic laser-textured surface at (a) 0.001 wt.% and (b) 0.1 wt.% concentrations of TiO₂ nanoparticles.

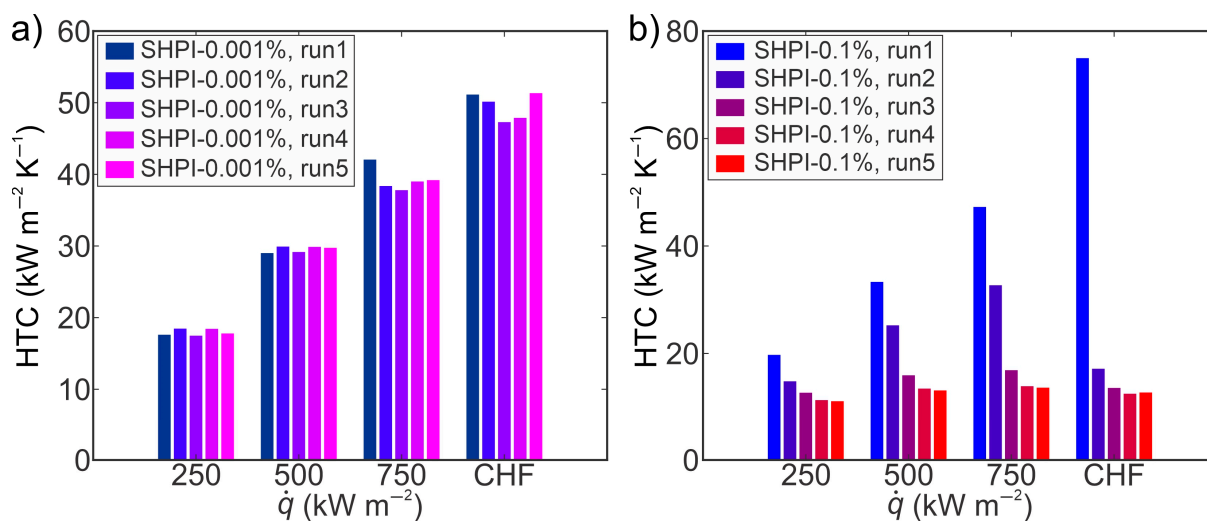


Figure 8. Heat transfer coefficients of TiO₂–water nanofluid on a superhydrophilic laser-textured surface at (a) 0.001 wt.% and (b) 0.1 wt.% concentrations of TiO₂ nanoparticles.

Corroborating this, the conducted SEM analysis (Figure 9) demonstrates that a very thin deposited layer of TiO₂ nanoparticles persists on the laser-engineered structure after five hours of boiling at 0.001 wt.% and is only evident at higher magnifications. Conversely, during boiling at higher concentrations (0.1 wt.%), the deposited nanoparticles on the surface manifest more evidently, filling a substantial portion of the laser-engineered surface channels and forming a thicker nanoparticle layer. Thickening of the deposit on the surface results in additional thermal resistance, which can also result in the deterioration of the heat transfer coefficient. Similar observations of the effect of concentration on the deposited layer and further on boiling performance can be found in the literature [27,55,56].

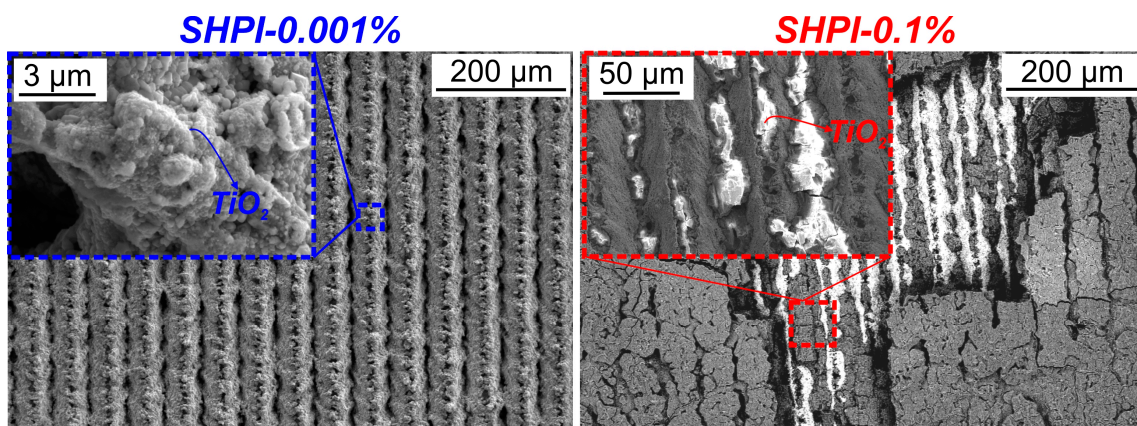


Figure 9. SEM images of superhydrophilic samples after boiling at concentrations of 0.001 wt.% (left) and 0.1 wt.% (right).

3.3. Boiling Heat Transfer on Superhydrophobic Surfaces with TiO_2 –Water Nanofluid

The boiling performance of TiO_2 nanofluid (at concentrations of 0.001 wt.% and 0.1 wt.%) on superhydrophobic laser-engineered surfaces was assessed employing the same approach as that applied to their superhydrophilic counterparts. Five boiling curves were recorded up to CHF incipience for both concentrations, resulting in five-hour boiling tests for each concentration on superhydrophobic samples. The boiling curves corresponding to a concentration of 0.001 wt.% are shown in Figure 10a, while those for a concentration of 0.1 wt.% are illustrated in Figure 10b. It was observed that the boiling curves acquired on superhydrophobic surfaces with nanofluids were unstable, exhibiting a shift toward higher superheats after the initial experimental run. The shift of boiling curves with each consecutive run is the result of a decrease in nucleation site density that can be attributed to the deposition of nanoparticles that were filling the microcavities. The CHF values demonstrated an upward trend from the first to the fifth run on superhydrophobic surfaces at both concentrations, achieving the most substantial increase of 19% at 0.1 wt%. This increase in CHF is ascribed to a thicker and more porous layer that formed on superhydrophobic surfaces due to the deposition of hydrophilic TiO_2 nanoparticles with each following run. The deposited hydrophilic nanoparticles covering the superhydrophobic surface result in the transition of wetting from superhydrophobicity towards hydrophilicity. The latter was confirmed by contact angle measurements after boiling, where the SHPO surface after boiling in a higher nanofluid concentration exhibited a contact angle of 20° , while after boiling in 0.001 wt.%, an average apparent contact angle of 79° was measured. Hydrophilic porous boiling interface induces an increase in liquid supply towards dry spots during bubble departures, universally enhancing the critical heat flux by mitigating dryout spots [57,58]. Nonetheless, in comparison with their superhydrophilic counterparts, superhydrophobic surfaces manifested lower CHF values after five consecutive runs at both tested concentrations. This observation aligns with findings from boiling studies on superhydrophilic and superhydrophobic surfaces with water, where it is well-established that superhydrophilic surfaces tend to delay dryout and augment CHF, whereas poorly wettable surfaces (superhydrophobic) typically fail to impede bubble coalescence, leading to the transition into film boiling at lower heat flux values [43,59,60].

The HTC values during nanofluid boiling on superhydrophobic surfaces at various heat flux levels are presented in Figure 11. The highest HTCs were observed during the first run at a heat flux near the CHF for both tested concentrations. Specifically, at 0.001 wt.%, the maximum HTC reached $96 \text{ kW m}^{-2} \text{ K}^{-1}$, signifying an 88% enhancement over its superhydrophilic counterpart. Subsequent experimental runs revealed a decrease in HTC values towards the fifth run at both concentrations, attributed to nanoparticle deposition on surfaces. The deposition of nanoparticles in laser-induced microcavities resulted in decreased nucleation site density, thereby deteriorating the heat transfer coefficient. At

0.1 wt.%, the most substantial decrease in HTC, 75% from the first to the fifth run, was observed, which is 10% less than that observed on the superhydrophilic counterpart. The decrease in HTC on superhydrophobic surfaces can be ascribed to the hydrophobic coating, potentially mitigating nanoparticle deposition on the laser structure, thereby lowering the decrease in nucleation site density and lowering the HTC deterioration. A detailed discussion on the impact of superhydrophobic coating on the mitigation of nanoparticle deposition onto structured surfaces is provided in the subsequent section. Furthermore, a comparative analysis of results obtained with nanofluids on superhydrophobic surfaces and water on reference surfaces reveals improvements in HTC and CHF of up to 90% and 20%, respectively. This enhancement is predominantly attributed to laser-induced cavities on surfaces rather than the addition of nanoparticles to the base fluid.

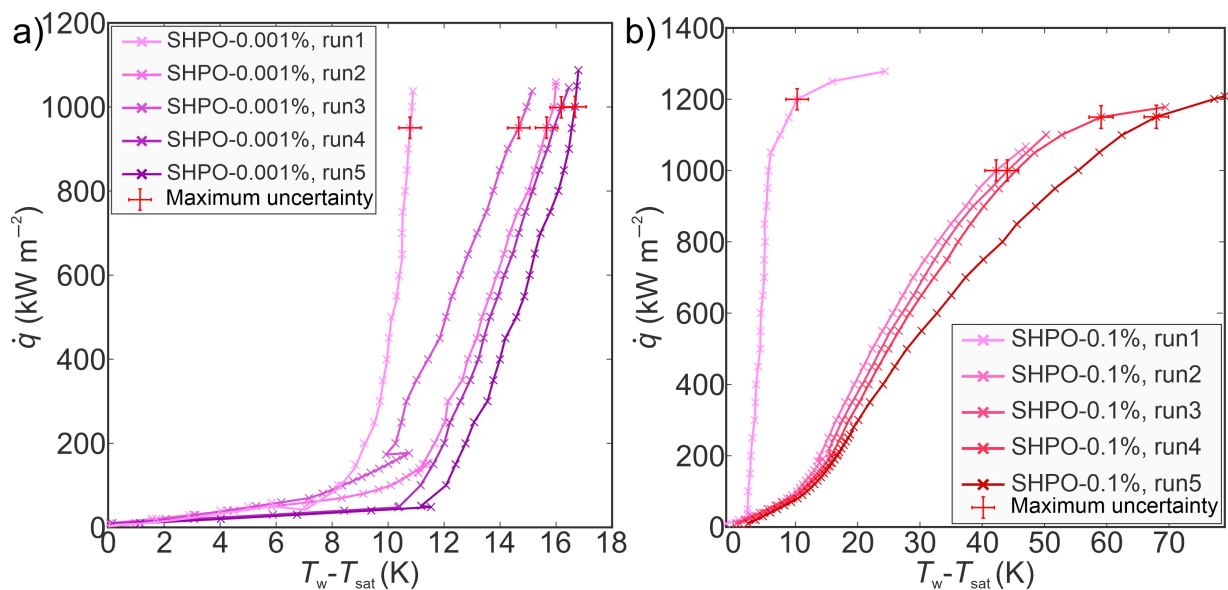


Figure 10. Boiling curves of TiO₂–water nanofluid on a superhydrophobic laser-textured surface at (a) 0.001 wt.% and (b) 0.1 wt.% concentrations of TiO₂ nanoparticles.

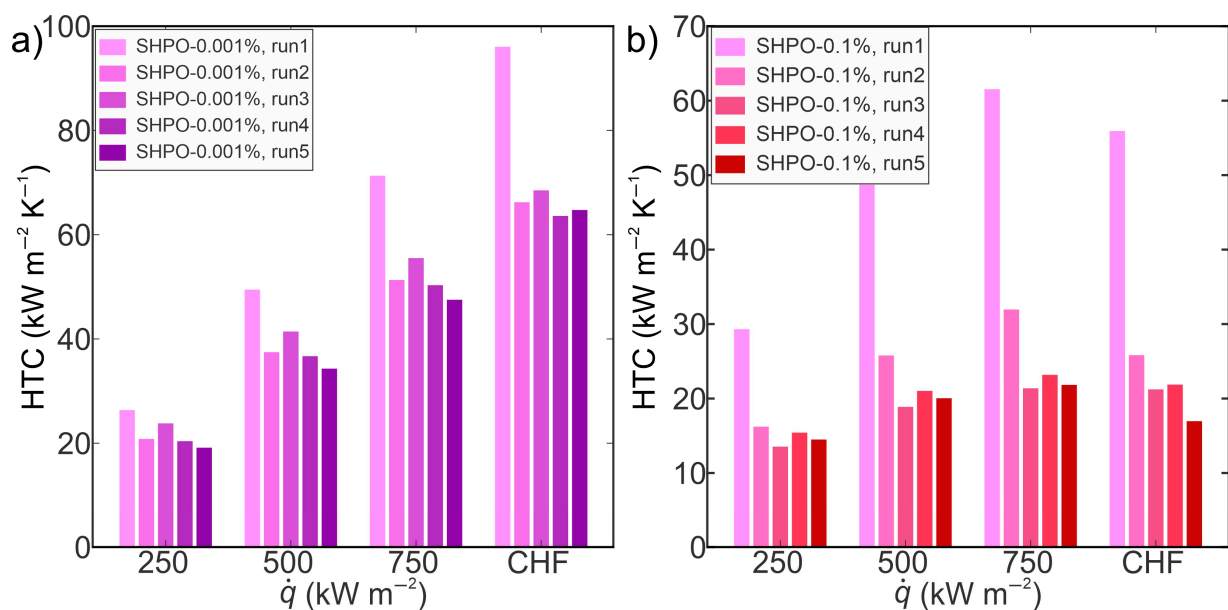


Figure 11. Heat transfer coefficients of TiO₂–water nanofluid on a superhydrophobic laser-textured surface at (a) 0.001 wt.% and (b) 0.1 wt.% concentrations of TiO₂ nanoparticles.

Furthermore, SEM images presented in Figure 12 show that the deposition of a thicker layer of nanoparticles occurred on the superhydrophobic (SHPO) sample subjected to boiling at a higher concentration, in contrast to the sample subjected to a lower concentration. The observed augmentation in the thickness of the TiO₂-deposited nanoparticle layer on superhydrophobic surfaces is concomitant with an increase in nanoparticle concentration, which is an analogous trend observed in superhydrophilic samples. As previously mentioned, the larger thickness of the nanoparticle layer may induce greater thermal resistance, thereby resulting in a more pronounced degradation of boiling performance.

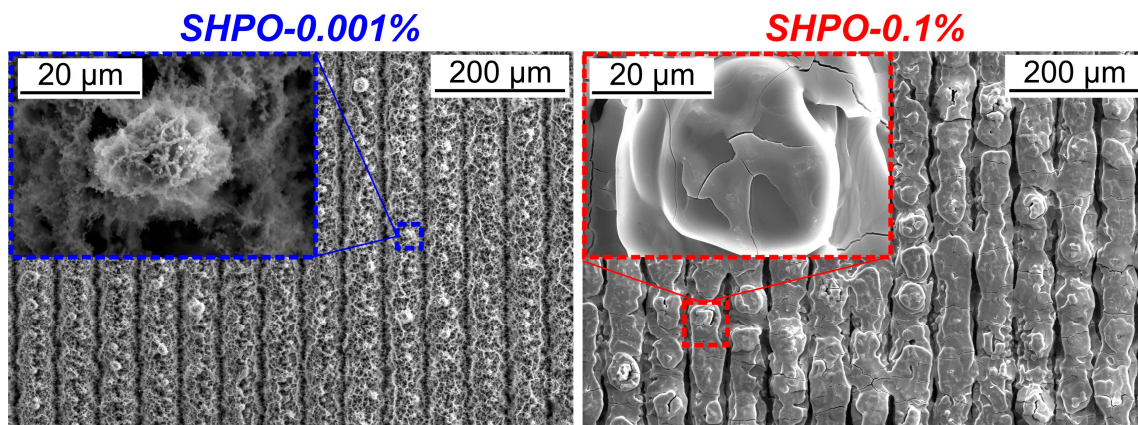


Figure 12. SEM images of superhydrophobic samples after boiling at concentrations of 0.001 wt.% (left) and 0.1 wt.% (right).

3.4. Nanoparticle Deposition and Its Influence on Boiling Heat Transfer

From observations noted in previous sections, one can observe the similarities between the boiling of nanofluids and particulate fouling during nucleate pool boiling. Clearly, the local deposition of nano-sized particular matter onto the modified topography plays a key role in measurable changes in overall pool boiling performance with time. The latter can best be characterized by a shift of the pool boiling curve to higher superheats, which is to an extent also influenced by: (i) the stochastic nature of nucleation site activation/deactivation after each run; (ii) the CHF-induced changes to surface morphology (note the improvement in performance of the SHPI sample in water after the first CHF incipience due to oxide transformations); and (iii) the dynamic testing procedure affecting deposition. Hence, to reduce these influences, the mean wall superheat was computed in the heat flux region between 50 kW m^{-2} and 900 kW m^{-2} for all tested surface-fluid combinations (see Figure 13). In this way, one can more accurately compare the boiling curve shifts, which are indicative of performance degradation (or improvement) and thus correlated to nanoparticle deposition. The values clearly show the impact of nanoparticle deposition (or lack thereof) on surface temperature changes for all the tested surface-fluid combinations. The SHPI and SHPO samples exhibited a small shift of -3.5 K and $+0.2 \text{ K}$ after the five tests in pure water, respectively, which indicates that changes are not induced only by deposition. However, in the absence of a deposit-forming element, these shifts are minimal or even beneficial (towards lower superheats). When nanoparticles are present, the smaller concentration of 0.001wt.% appears to influence the SHPO surface to a larger extent ($+4.5 \text{ K}$ shift, compared to the $+1.2 \text{ K}$ shift of the SHPI sample), which may originate from the more pronounced change of wetting of the SHPO surface. The transition towards its improved wetting points to an increase in surface energy, which increases the energy barrier for nucleation and results in bubble formation at a higher surface superheat [61]. On the other hand, the SHPI sample's wettability changes to a much smaller extent. The latter observations indicate that, at very low nanoparticle concentrations, the dominant influence on boiling curve shifts appears not to be the added thermal resistance of the deposit

but instead the change in wetting properties, correlated to the deposit accumulation and oxide growth.

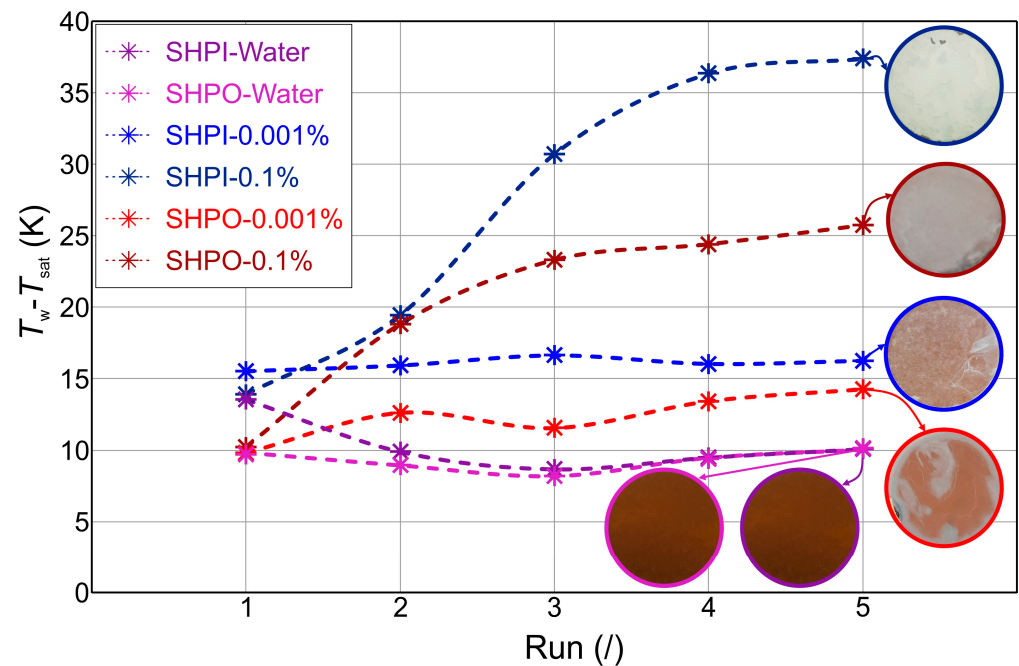


Figure 13. Nanoparticle deposition-induced changes, characterized by mean pool boiling curve wall temperature in the heat flux range of $50\text{--}900\text{ kW m}^{-2}$ and corresponding sample surface images. Plots of samples boiled in clean water are included to serve as a reference and point out that boiling performance also changes in clean water, where no deposition was observed.

On the contrary, when both samples were tested in a nanofluid of 0.1 wt.%, the respective shifts of +23.5 K and +15.5 K were much more pronounced, pointing towards a larger and dominant effect of added thermal resistance, originating from a thick deposit layer that covered the surface (see SEM micrographs in Figures 9 and 12). In respect to this, the SHPO surface degraded slower and to a smaller extent, pointing towards improved mitigation of surface deposition, as also evident by less surface discoloration (see sample images in Figure 13). This may be attributed to the weaker adhesion of particles to the SHPO sample with low surface energy, as well as to the distinct features of superhydrophobic nano- and microstructured surfaces. Namely, the trapped gas and vapor content within such surface structures is much higher than within their unhydrophobized counterpart, acting as a mitigative blanket against deposition. The increased affinity towards the gaseous phase promotes bubble nucleation, resulting in vigorous lateral and vertical coalescence of many small and fast-forming bubbles over the surface. Consequently, near-wall turbulence and shear stress are increased, which has previously been shown to mitigate particulate deposition [19].

The discussion above is especially relevant when considering a combination of nanoparticles and boiling surface materials, where the latter has a higher thermal conductivity than the former, such as the combination used in this study. In such cases, it is critical to mitigate the deposition of nanoparticles as much as possible to avoid inducing a large thermal resistance. In contrast, if highly conductive nanoparticles were used, the deposition-mitigative feature would likely have a smaller influence, which will be the focus of our future studies.

4. Conclusions

The pool boiling performance of TiO_2 -water nanofluids at two distinct concentrations (0.001 wt.% and 0.1 wt.%) was studied on laser-engineered surfaces in superhydrophilic

and superhydrophobic states. The following conclusions were drawn based on the obtained experimental results:

1. Superhydrophobic and superhydrophilic laser-engineered surfaces exhibited an HTC enhancement of up to 120% over the reference surface due to fabricated microcavities that led to increased nucleation site density.
2. The boiling of nanofluids on functionalized (i.e., superhydrophilic and superhydrophobic laser-engineered) surfaces failed to provide an additional improvement in the HTC compared to boiling pure water.
3. At a low nanoparticle concentration, the influence of nanofluid on boiling performance is minimal, with CHF values comparable to those obtained using pure water on both the untreated, superhydrophilic and superhydrophobic laser-textured surfaces. On the other hand, at a high nanoparticle concentration, superhydrophobic and superhydrophilic laser-textured surfaces exhibited CHF enhancement up to 30% over their counterparts tested with pure water.
4. Boiling performance changes can be connected to nanoparticle deposition on the surface, where the superhydrophobic surface outperforms its non-hydrophobized counterpart at high concentrations. The influence of deposit-induced added thermal resistance is smaller at low nanofluid concentrations, and instead, the changes appear to be governed by a deposit-induced wettability transition.

Author Contributions: Conceptualization, I.G. and H.G.; methodology, M.M. and J.B.; software, M.M., J.B. and M.Z.; validation, I.G., H.G. and M.Z.; formal analysis, K.A., A.H. and J.B.; investigation, J.B. and A.H.; resources, I.G.; data curation, M.M. and K.A.; writing—original draft preparation, A.H., K.A. and J.B.; writing—review and editing, M.M. and J.B.; visualization, A.H., K.A. and J.B.; supervision, H.G., M.Z. and I.G.; project administration, I.G.; funding acquisition, I.G. and M.Z. All authors have read and agreed to the published version of the manuscript.

Funding: The authors acknowledge the financial support from the state budget of the Slovenian Research Agency (Program No. P2-0223 and Project Nos. J2-50085 and N2-0251).

Data Availability Statement: Data are available from the authors upon reasonable request.

Conflicts of Interest: The authors declare no conflicts of interest.

References

1. Liang, G.; Chen, Y.; Yang, H.; Li, D.; Shen, S. Nucleate Boiling Heat Transfer and Critical Heat Flux (CHF) from Micro-Pit Surfaces. *Int. J. Heat Mass Transf.* **2020**, *152*, 119510. [[CrossRef](#)]
2. Rahimian, A.; Kazeminejad, H.; Khalafi, H.; Akhavan, A.; Mirvakili, S.M. Boiling Heat Transfer and Critical Heat Flux Enhancement Using Electrophoretic Deposition of SiO₂ Nanofluid. *Sci. Technol. Nucl. Install.* **2019**, *2019*, 1272156. [[CrossRef](#)]
3. Hernandez, R.; Folsom, C.P.; Woolstenhulme, N.E.; Jensen, C.B.; Bess, J.D.; Gorton, J.P.; Brown, N.R. Review of Pool Boiling Critical Heat Flux (CHF) and Heater Rod Design for CHF Experiments in TREAT. *Prog. Nucl. Energy* **2020**, *123*, 103303. [[CrossRef](#)]
4. Ahn, H.S.; Sathyamurthi, V.; Banerjee, D. Pool Boiling Experiments on a Nano-Structured Surface. *IEEE Trans. Components Packag. Technol.* **2009**, *32*, 156–165. [[CrossRef](#)]
5. Rahman, M.M.; McCarthy, M. Boiling Enhancement on Nanostructured Surfaces with Engineered Variations in Wettability and Thermal Conductivity. *Heat Transf. Eng.* **2017**, *38*, 1285–1295. [[CrossRef](#)]
6. Barber, J.; Brutin, D.; Tadrist, L. A Review on Boiling Heat Transfer Enhancement with Nanofluids. *Nanoscale Res. Lett.* **2011**, *6*, 280. [[CrossRef](#)] [[PubMed](#)]
7. Song, S.L.; Lee, J.H.; Chang, S.H. CHF Enhancement of SiC Nanofluid in Pool Boiling Experiment. *Exp. Therm. Fluid Sci.* **2014**, *52*, 12–18. [[CrossRef](#)]
8. Hu, H.; Xu, C.; Zhao, Y.; Shaeffer, R.; Ziegler, K.J.; Chung, J.N. Modification and Enhancement of Cryogenic Quenching Heat Transfer by a Nanoporous Surface. *Int. J. Heat Mass Transf.* **2015**, *80*, 636–643. [[CrossRef](#)]
9. Cai, Z.; Wang, B.; Liu, S.; Li, H.; Luo, S.; Dong, Z.; Wang, Y. Enhancing Boiling Heat Transfer on a Superheated Surface by Surfactant-Laden Droplets. *Langmuir* **2022**, *38*, 10375–10384. [[CrossRef](#)]
10. Kong, D.; Kang, M.; Kim, K.Y.; Jang, J.; Cho, J.; In, J.B.; Lee, H. Hierarchically Structured Laser-Induced Graphene for Enhanced Boiling on Flexible Substrates. *ACS Appl. Mater. Interfaces* **2020**, *12*, 37784–37792. [[CrossRef](#)]
11. Gouda, R.K.; Pathak, M.; Khan, M.K. Pool Boiling Heat Transfer Enhancement with Segmented Finned Microchannels Structured Surface. *Int. J. Heat Mass Transf.* **2018**, *127*, 39–50. [[CrossRef](#)]

12. Song, Y.; Gong, S.; Vaartstra, G.; Wang, E.N. Microtube Surfaces for the Simultaneous Enhancement of Efficiency and Critical Heat Flux during Pool Boiling. *ACS Appl. Mater. Interfaces* **2021**, *13*, 12629–12635. [[CrossRef](#)]
13. Mudawar, I. Recent Advances in High-Flux, Two-Phase Thermal Management. *J. Therm. Sci. Eng. Appl.* **2013**, *5*, 021012. [[CrossRef](#)]
14. Smakulski, P.; Pietrowicz, S. A Review of the Capabilities of High Heat Flux Removal by Porous Materials, Microchannels and Spray Cooling Techniques. *Appl. Therm. Eng.* **2016**, *104*, 636–646. [[CrossRef](#)]
15. Liang, G.; Mudawar, I. Review of Pool Boiling Enhancement with Additives and Nanofluids. *Int. J. Heat Mass Transf.* **2018**, *124*, 423–453. [[CrossRef](#)]
16. Taylor, R.A.; Phelan, P.E. Pool Boiling of Nanofluids: Comprehensive Review of Existing Data and Limited New Data. *Int. J. Heat Mass Transf.* **2009**, *52*, 5339–5347. [[CrossRef](#)]
17. Kim, H. Enhancement of Critical Heat Flux in Nucleate Boiling of Nanofluids: A State-of-Art Review. *Nanoscale Res. Lett.* **2011**, *6*, 415. [[CrossRef](#)]
18. Berce, J.; Zupančič, M.; Može, M.; Golobič, I. Infrared Thermography Observations of Crystallization Fouling in a Plate Heat Exchanger. *Appl. Therm. Eng.* **2023**, *224*, 120116. [[CrossRef](#)]
19. Peyghambarzadeh, S.M.; Vatani, A.; Jamialahmadi, M. Influences of Bubble Formation on Different Types of Heat Exchanger Fouling. *Appl. Therm. Eng.* **2013**, *50*, 848–856. [[CrossRef](#)]
20. Ciloglu, D.; Bolukbasi, A. A Comprehensive Review on Pool Boiling of Nanofluids. *Appl. Therm. Eng.* **2015**, *84*, 45–63. [[CrossRef](#)]
21. Manetti, L.L.; Stephen, M.T.; Beck, P.A.; Cardoso, E.M. Evaluation of the Heat Transfer Enhancement during Pool Boiling Using Low Concentrations of Al₂O₃-Water Based Nanofluid. *Exp. Therm. Fluid Sci.* **2017**, *87*, 191–200. [[CrossRef](#)]
22. Suriyawong, A.; Wongwises, S. Nucleate Pool Boiling Heat Transfer Characteristics of TiO₂-Water Nanofluids at Very Low Concentrations. *Exp. Therm. Fluid Sci.* **2010**, *34*, 992–999. [[CrossRef](#)]
23. Santos, R.; Moita, A.S.; Ribeiro, A.P.C.; Moreira, A.L.N. The Impact of Alumina Nanofluids on Pool Boiling Performance on Biphilic Surfaces for Cooling Applications. *Energies* **2022**, *15*, 372. [[CrossRef](#)]
24. Peng, H.; Ding, G.; Hu, H.; Jiang, W. Effect of Nanoparticle Size on Nucleate Pool Boiling Heat Transfer of Refrigerant/Oil Mixture with Nanoparticles. *Int. J. Heat Mass Transf.* **2011**, *54*, 1839–1850. [[CrossRef](#)]
25. Kiyomura, I.S.; Manetti, L.L.; da Cunha, A.P.; Ribatski, G.; Cardoso, E.M. An Analysis of the Effects of Nanoparticles Deposition on Characteristics of the Heating Surface and ON Pool Boiling of Water. *Int. J. Heat Mass Transf.* **2017**, *106*, 666–674. [[CrossRef](#)]
26. Kim, H.; Buongiorno, J.; Hu, L.W.; McKrell, T. Nanoparticle Deposition Effects on the Minimum Heat Flux Point and Quench Front Speed during Quenching in Water-Based Alumina Nanofluids. *Int. J. Heat Mass Transf.* **2010**, *53*, 1542–1553. [[CrossRef](#)]
27. Huang, C.K.; Lee, C.W.; Wang, C.K. Boiling Enhancement by TiO₂ Nanoparticle Deposition. *Int. J. Heat Mass Transf.* **2011**, *54*, 4895–4903. [[CrossRef](#)]
28. Fang, X.; Chen, Y.; Zhang, H.; Chen, W.; Dong, A.; Wang, R. Heat Transfer and Critical Heat Flux of Nanofluid Boiling: A Comprehensive Review. *Renew. Sustain. Energy Rev.* **2016**, *62*, 924–940. [[CrossRef](#)]
29. Hadžić, A.; Može, M.; Arhar, K.; Zupančič, M.; Golobič, I. Effect of Nanoparticle Size and Concentration on Pool Boiling Heat Transfer with TiO₂ Nanofluids on Laser-Textured Copper Surfaces. *Nanomaterials* **2022**, *12*, 2611. [[CrossRef](#)] [[PubMed](#)]
30. Dadhich, M.; Prajapati, O.S. A Brief Review on Factors Affecting Flow and Pool Boiling. *Renew. Sustain. Energy Rev.* **2019**, *112*, 607–625. [[CrossRef](#)]
31. Rishi, A.M.; Gupta, A.; Kandlikar, S.G. Improving Aging Performance of Electrodeposited Copper Coatings during Pool Boiling. *Appl. Therm. Eng.* **2018**, *140*, 406–414. [[CrossRef](#)]
32. Patil, C.M.; Santhanam, K.S.V.; Kandlikar, S.G. Development of a Two-Step Electrodeposition Process for Enhancing Pool Boiling. *Int. J. Heat Mass Transf.* **2014**, *79*, 989–1001. [[CrossRef](#)]
33. Može, M.; Hadžić, A.; Zupančič, M.; Golobič, I. Boiling Heat Transfer Enhancement on Titanium through Nucleation-Promoting Morphology and Tailored Wettability. *Int. J. Heat Mass Transf.* **2022**, *195*, 123161. [[CrossRef](#)]
34. Serdyukov, V.; Starinskiy, S.; Malakhov, I.; Safonov, A.; Surtaev, A. Laser Texturing of Silicon Surface to Enhance Nucleate Pool Boiling Heat Transfer. *Appl. Therm. Eng.* **2021**, *194*, 117102. [[CrossRef](#)]
35. Ta, D.V.; Dunn, A.; Wasley, T.J.; Kay, R.W.; Stringer, J.; Smith, P.J.; Connaughton, C.; Shephard, J.D. Nanosecond Laser Textured Superhydrophobic Metallic Surfaces and Their Chemical Sensing Applications. *Appl. Surf. Sci.* **2015**, *357*, 248–254. [[CrossRef](#)]
36. Liang, G.; Mudawar, I. Review of Pool Boiling Enhancement by Surface Modification. *Int. J. Heat Mass Transf.* **2019**, *128*, 892–933. [[CrossRef](#)]
37. Ranjan, A.; Ahmad, I.; Gouda, R.K.; Pathak, M.; Khan, M.K. Enhancement of Critical Heat Flux (CHF) in Pool Boiling with Anodized Copper Surfaces. *Int. J. Therm. Sci.* **2022**, *172*, 107338. [[CrossRef](#)]
38. Ranjan, A.; Priy, A.; Ahmad, I.; Pathak, M.; Khan, M.K. Pool Boiling Heat Transfer Characteristics of a Stepped Microchannel Structured Heating Surface. *Int. J. Multiph. Flow* **2023**, *160*, 104351. [[CrossRef](#)]
39. Sujith Kumar, C.S.; Udaya Kumar, G.; Mata Arenales, M.R.; Hsu, C.C.; Suresh, S.; Chen, P.H. Elucidating the Mechanisms behind the Boiling Heat Transfer Enhancement Using Nano-Structured Surface Coatings. *Appl. Therm. Eng.* **2018**, *137*, 868–891. [[CrossRef](#)]
40. Može, M.; Senegačnik, M.; Gregorčič, P.; Hočevar, M.; Zupančič, M.; Golobič, I. Laser-Engineered Microcavity Surfaces with a Nanoscale Superhydrophobic Coating for Extreme Boiling Performance. *ACS Appl. Mater. Interfaces* **2020**, *12*, 24419–24431. [[CrossRef](#)] [[PubMed](#)]

41. Allred, T.P.; Weibel, J.A.; Garimella, S.V. Enabling Highly Effective Boiling from Superhydrophobic Surfaces. *Phys. Rev. Lett.* **2018**, *120*, 174501. [[CrossRef](#)]
42. Motezakker, A.R.; Sadaghiani, A.K.; Çelik, S.; Larsen, T.; Villanueva, L.G.; Koşar, A. Optimum Ratio of Hydrophobic to Hydrophilic Areas of Bipilic Surfaces in Thermal Fluid Systems Involving Boiling. *Int. J. Heat Mass Transf.* **2019**, *135*, 164–174. [[CrossRef](#)]
43. Hadžić, A.; Može, M.; Zupančič, M.; Golobič, I. Superbiphilic Laser-Microengineered Surfaces with A Self-Assembled Monolayer Coating for Exceptional Boiling Performance. *Adv. Funct. Mater.* **2023**, *2310662*, 1–14. [[CrossRef](#)]
44. Serdyukov, V.; Patrin, G.; Malakhov, I.; Surtaev, A. Bipilic Surface to Improve and Stabilize Pool Boiling in Vacuum. *Appl. Therm. Eng.* **2022**, *209*, 118298. [[CrossRef](#)]
45. Teodori, E.; Palma, T.; Valente, T.; Moita, A.S.; Moreira, A.L.N. Bubble Dynamics and Heat Transfer for Pool Boiling on Hydrophilic, Superhydrophobic and Bipilic Surfaces. *J. Phys. Conf. Ser.* **2016**, *745*, 032132. [[CrossRef](#)]
46. Coursey, J.S.; Kim, J. Nanofluid Boiling: The Effect of Surface Wettability. *Int. J. Heat Fluid Flow* **2008**, *29*, 1577–1585. [[CrossRef](#)]
47. Freitas, E.; Pontes, P.; Cautela, R.; Bahadur, V.; Miranda, J.; Ribeiro, A.P.C.; Souza, R.R.; Oliveira, J.D.; Copetti, J.B.; Lima, R.; et al. Article Pool Boiling of Nanofluids on Bipilic Surfaces: An Experimental and Numerical Study. *Nanomaterials* **2021**, *11*, 125. [[CrossRef](#)] [[PubMed](#)]
48. Ji, W.-T.; Zhao, P.-F.; Zhao, C.-Y.; Ding, J.; Tao, W.-Q. Pool Boiling Heat Transfer of Water and Nanofluid Outside the Surface with Higher Roughness and Different Wettability. *Nanoscale Microscale Thermophys. Eng.* **2018**, *22*, 296–323. [[CrossRef](#)]
49. Može, M.; Vajc, V.; Zupančič, M.; Golobič, I. Hydrophilic and Hydrophobic Nanostructured Copper Surfaces for Efficient Pool Boiling Heat Transfer with Water, Water/Butanol Mixtures and Novec 649. *Nanomaterials* **2021**, *11*, 3216. [[CrossRef](#)] [[PubMed](#)]
50. Može, M.; Zupančič, M.; Golobič, I. Investigation of the Scatter in Reported Pool Boiling CHF Measurements Including Analysis of Heat Flux and Measurement Uncertainty Evaluation Methodology. *Appl. Therm. Eng.* **2020**, *169*, 114938. [[CrossRef](#)]
51. Mahamudur Rahman, M.; Pollack, J.; Mccarthy, M. Increasing Boiling Heat Transfer Using Low Conductivity Materials. *Sci. Rep.* **2015**, *5*, 12–14. [[CrossRef](#)]
52. Kruse, C.M.; Anderson, T.; Wilson, C.; Zuhlke, C.; Alexander, D.; Gogos, G.; Ndao, S. Enhanced Pool-Boiling Heat Transfer and Critical Heat Flux on Femtosecond Laser Processed Stainless Steel Surfaces. *Int. J. Heat Mass Transf.* **2015**, *82*, 109–116. [[CrossRef](#)]
53. Može, M.; Zupančič, M.; Hočevar, M.; Golobič, I.; Gregorčič, P. Surface Chemistry and Morphology Transition Induced by Critical Heat Flux Incipience on Laser-Textured Copper Surfaces. *Appl. Surf. Sci.* **2019**, *490*, 220–230. [[CrossRef](#)]
54. Truong, B.H. Determination of Pool Boiling Critical Heat Flux Enhancement in Nanofluids. In Proceedings of the ASME International Mechanical Engineering Congress and Exposition, Seattle, WA, USA, 11–15 November 2007; pp. 289–299.
55. Park, S.D.; Moon, S.B.; Bang, I.C. Effects of Thickness of Boiling-Induced Nanoparticle Deposition on the Saturation of Critical Heat Flux Enhancement. *Int. J. Heat Mass Transf.* **2014**, *78*, 506–514. [[CrossRef](#)]
56. Khan, A.; Ali, H.M. A Comprehensive Review Pool Boiling Using Nanofluids. *Therm. Sci.* **2019**, *23*, 3209–3237. [[CrossRef](#)]
57. Mori, S.; Mt Aznam, S.; Okuyama, K. Enhancement of the Critical Heat Flux in Saturated Pool Boiling of Water by Nanoparticle-Coating and a Honeycomb Porous Plate. *Int. J. Heat Mass Transf.* **2015**, *80*, 1–6. [[CrossRef](#)]
58. Li, J.; Fu, W.; Zhang, B.; Zhu, G.; Miljkovic, N. Ultrascalable Three-Tier Hierarchical Nanoengineered Surfaces for Optimized Boiling. *ACS Nano* **2019**, *13*, 14080–14093. [[CrossRef](#)] [[PubMed](#)]
59. Betz, A.R.; Jenkins, J.; Kim, C.J.; Attinger, D. Boiling Heat Transfer on Superhydrophilic, Superhydrophobic, and Superbiphilic Surfaces. *Int. J. Heat Mass Transf.* **2013**, *57*, 733–741. [[CrossRef](#)]
60. Pontes, P.; Cautela, R.; Teodori, E.; Moita, A.S.; Moreira, A.L.N. Experimental Description of Bubble Dynamics and Heat Transfer Processes Occurring on the Pool Boiling of Water on Bipilic Surfaces. *Appl. Therm. Eng.* **2020**, *178*, 115507. [[CrossRef](#)]
61. Cole, R. Boiling Nucleation. *Adv. Heat Transf.* **1974**, *10*, 85–166.

Disclaimer/Publisher’s Note: The statements, opinions and data contained in all publications are solely those of the individual author(s) and contributor(s) and not of MDPI and/or the editor(s). MDPI and/or the editor(s) disclaim responsibility for any injury to people or property resulting from any ideas, methods, instructions or products referred to in the content.